Implementation and Model Verification of a Magnetic Levitation System

Robert Brydon Owen and Manfredi Maggiore

Abstract— This paper presents the implementation of a two degree-of-freedom magnetic levitation system employing one permanent magnet linear synchronous motor, and the experimental validation of a mathematical model previously derived. The paper focuses on showing the development of a calibration procedure to estimate model parameters and its subsequent use for model verification. Experimental results show that the proposed mathematical model accurately describes the dynamics of the system over a wide operating range showing promise for the future implementation of nonlinear controllers.

I. INTRODUCTION

In semiconductor manufacturing, many process stages require positioning systems, referred to as *microsteppers*, capable of several degrees of freedom (DOF) with significant speed and precision [1]. As the pace of technology causes the dimensions of semiconductors to further decrease, there is an increasing interest, in industry, to replace traditional mechanical microsteppers by contactless positioning devices. This arises from the fact that mechanical contacts introduce impurities that may limit the accuracy of the photo-lithographic process, thus decreasing production throughput. Further, mechanical positioning devices require costly maintenance due to the wear of their components.

In [2], Kim and Trumper proposed a contactless microstepper which employs single sided *air cored* permanent magnet linear synchronous motors (PMLSM) to actuate six degrees-of-freedom. Individually, PMLSMs produce both a normal and translational force with appropriate control. When several are combined in appropriate fashion, multiple degrees of freedom can be achieved. In [3], modelling and nonlinear control designs are presented for an idealized three degrees-of-freedom device which employs *iron cored* PMLSMs. This device was designed to work over a large range of operation and to employ standard PMLSMs commonly found on the market.

This paper initiates the experimental verification of the theory developed in [3] using a simplified 2-DOF apparatus constructed by Quanser Consulting. We use a parameter identification technique developed in [4] to estimate the parameters of the model in [3] and then compare the behavior predicted by the model to what is actually observed. Such

The authors are with the Edward S. Rogers Department of Electrical and Computer Engineering, University of Toronto, 10 King's College Road, Toronto, ON M5S 3G4, Canada. bowen@control.toronto.edu maggiore@control.toronto.edu

comparison demonstrates accuracy of the model over a wide range of operation (100 mm $\times$10 mm). Future work will focus on the implementation of nonlinear controllers based on the designs in [3].

We begin our discussion with a description of the magnetic levitation hardware utilized during experimentation, along with a brief summary of the model derivation. This is followed by the parameter identification technique found in [4]. The actual model verification procedure is then presented in conjunction with a series of experimental results. The paper concludes with a description of future extensions to the magnetic levitation implementation.

II. DESCRIPTION OF 2-DOF HARDWARE

A photo of the 2-DOF hardware implementation is shown in Figure 1. As mentioned earlier, we employ a single sided iron-cored PMLSM.

Fig. 1.   2-DOF magnetic levitation hardware implementation

The *stator* of the PMLSM, which is fixed in place to a heavy aluminium frame, is longitudinally laminated and transversally slotted in order to accommodate a single layer of 3-phase winding. The *mover,* which is attached to two orthogonally mounted linear guides allowing for horizontal and vertical movement, is composed of a set of four type N35 permanent magnets (PM) attached to a ferromagnetic backing. The details of the hardware specifications are summarized in Table I.

The 3-phase AC current required to actuate the stator coils is provided by a set of three linear current amplifier modules (LCAM) which are sent commands via a PC. The horizontal and vertical position information is provided to the PC by two linear optical encoders with a resolution of 10 μm. Controllers are implemented using the WINCON real-time code generator with Simulink as an interface.

TABLE I

SPECIFICATIONS FOR 2-DOF MAGNETIC LEVITATION HARDWARE

Parameter	Symbol	units	value
Stator slot width	b_0	mm	12.7
Stator slot pitch	t_1	mm	19.05
Turns per phase	W	–	900
Coil pitch	ω_c	mm	57.15
Stator pole pairs	p	–	3
Number of stator slots	z_1	–	18
PM height	h_m	mm	5
PM length	L_A	mm	50
Number of PM's	p_m	–	4
Pole pitch	τ	mm	57.15
PM width	τ_p	mm	28.58
PM coercivity	H_c	A/m	875400
Back iron height	h_b	mm	4.7
Back iron width	–	mm	50
Back iron length	–	mm	200.0
Horizontal Mover Mass	M_h	Kg	1.594
Vertical Mover Mass	M_v	Kg	4.350

With the current setup, the 2-DOF magnetic levitation system has a horizontal range of approximately ± 50 mm and a vertical range of approximately ± 10 mm. The goal is to eventually design a nonlinear controller to obtain positioning and tracking accuracy of at least 0.1 mm over the above mentioned horizontal range and a vertical range of ± 5 mm with as much speed as possible.

III. MODEL OF 2-DOF SYSTEM

The following is a brief summary of the model derivation applied to the 2-DOF system. The details of the modelling are found in [3].

Consider the inertial frame of the single PMLSM that forms the basis of the 2-DOF system, which is shown in Figure 2. Let L_A be the depth of each PM along the z axis, h_m be the height of the magnets, p_m the number of PM's, g the air-gap length, t_1 the slot pitch, b_0 the slot aperture, τ the PM pole pitch, τ_p the PM pole arc, μ_{rec} the relative PM recoil permeability, and σ_m the surface magnetic charge. To account for the effects of the stator slots, replace the air-gap g by the effective air-gap g_e, with $g_e = gK_c$, where K_c denotes Carter's coefficient. In addition, let $\mathbf{I}_a$, $\mathbf{I}_b$, and $\mathbf{I}_c$ be the phasors of the phase currents and I_a, I_b, and I_c their magnitudes. Define W to be the number of turns of wire on each phase, p the number of pole pairs in the stator, w_c the coil pitch, and k_{w1} the winding factor.

We define the horizontal motion to be along the x-axis while vertical motion is fixed to the y-axis. Defining G as the gravitational acceleration and M_h and M_v as the horizontal and vertical masses of the platform to be levitated[1], the following 2-DOF system model is obtained

$$
\begin{aligned}
\dot{x}_1 &= x_2, \\
\dot{x}_2 &= G - L_4(x_1)[u_1^2 + u_2^2] - L_3(x_1)u_2 - L_2(x_1), \\
\dot{x}_3 &= x_4, \\
\dot{x}_4 &= -L_1(x_1)u_1,
\end{aligned} \quad (1)
$$

[1]The horizontal and vertical masses of the platform are different due to the design of the 2-DOF apparatus
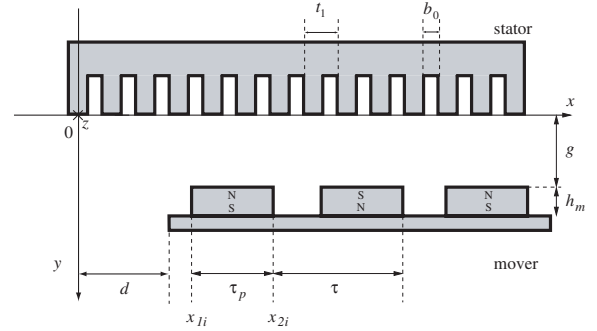

Fig. 2. Inertial frame of a single PMLSM

where

$$
\begin{aligned}
&x = [g, \dot{g}, d, \dot{d}]^T, \ u = [i_q, i_d]^T, \\
&L_1(x_1) = \frac{K_1(x_1)}{M_h}, \\
&L_i(x_1) = \frac{K_i(x_1)}{M_v}, \ i = 2, \dots, 4, \\
&K_1(x_1) = \frac{12\sqrt{2}Wk_{w1}p_mL_A\sigma_m\mu_0\tilde{\lambda}(x_1)\sinh(\frac{\pi}{\tau}h_m)\sin(\frac{\pi\tau_p}{2\tau})}{\pi pK_c(x_1)\sinh(\frac{\pi}{\tau}(h_m+x_1))}, \\
&K_2(x_1) = \frac{\tilde{\lambda}(x_1)L_Ap_m\tau B_{pmy1}(x_1)^2}{4\mu_0}, \\
&K_3(x_1) = -\frac{\tilde{\lambda}(x_1)3\sqrt{2}L_Ap_mWk_{w1}B_{pmy1}(x_1)\coth(\frac{\pi}{\tau}(h_m+x_1))}{p^2K_c(x_1)}, \\
&K_4(x_1) = \frac{\tilde{\lambda}(x_1)18L_Ap_mW^2k_{w1}^2\mu_0\coth^2(\frac{\pi}{\tau}(h_m+x_1))}{\tau p^2K_c(x_1)^2}, \\
&\tilde{\lambda}(x_1) = 1 - \frac{b_0^2}{4t_1(x_1+\frac{b_0}{2}+\frac{h_m}{\mu_{rec}})} \ .
\end{aligned}
$$

The function $B_{pmy1}(x_1)$ represents the magnetic field produced by the PM's and is numerically approximated using a 12th degree polynomial. Furthermore, i_d and i_q represent the direct and quadrature current inputs to the PMLSM. They are related to the 3-phase currents as follows

$$
i_d = I_a cos(\frac{\pi}{\tau}x_3), \quad i_q = -I_a sin(\frac{\pi}{\tau}x_3).
$$

The above model does not account for friction, cogging forces, and end effects. It is necessary to verify to what extent such unmodeled effects can be neglected within a reasonable range of operation. This is done in the following.

IV. SYSTEM ID METHODOLOGY

We begin by lumping together all constant unknown (or not perfectly known) parameters and rewriting (1) as

$$
\begin{aligned}
\dot{x}_1 &= x_2, \\
\dot{x}_2 &= G - C_4\frac{\tilde{\lambda}(x_1)\coth^2(\frac{\pi}{\tau}(h_m+x_1))}{K_c^2(x_1)}[u_1^2 + u_2^2] \\
&\quad + C_3\frac{\tilde{\lambda}(x_1)B_{pmy1}(x_1)\coth(\frac{\pi}{\tau}(h_m+x_1))}{K_c(x_1)}u_2 \\
&\quad - C_2\tilde{\lambda}(x_1)B_{pmy1}(x_1)^2, \\
\dot{x}_3 &= x_4, \\
\dot{x}_4 &= -C_1\frac{\tilde{\lambda}(x_1)}{K_c(x_1)\sinh(\frac{\pi}{\tau}(h_m+x_1))}u_1,
\end{aligned} \quad (2)
$$

where $C_1, \ldots, C_4$ are lumped constants to be determined experimentally and have the following form

$$C_1 = \frac{12\sqrt{2}Wk_{w1}p_m L_A \sigma_m \mu_0 \sinh(\frac{\pi}{\tau}h_m)\sin(\frac{\pi\tau_p}{2\tau})}{M_h \pi p},$$
$$C_2 = \frac{L_A p_m \tau}{M_v 4\mu_0},$$
$$C_3 = \frac{3\sqrt{2}L_A p_m W k_{w1}}{M_v p^2},$$
$$C_4 = \frac{18 L_A p_m W^2 k_{w1}^2 \mu_0}{M_v \tau p^2}.$$

Noticing that $C_1, \ldots, C_4$ enter the model linearly, we employ the technique presented in [4] to estimate them. For the sake of illustration, in what follows we briefly review the parameter identification technique in [4].

Consider the nonlinear system

$$\dot{x} = A(x,u)\theta + b(x,u) + \omega(t), \quad x(0) = x_0,$$

where θ is a vector of constant unknown parameters, all functions are smooth, and $\omega(t)$ is an $\mathcal{L}_\infty$ disturbance. It is assumed that a noisy measurement of the state x is available,

$$y = x + \varepsilon\nu(t),$$

where $\nu(t)$ is the measurement disturbance and ε is a known scalar. The value of ε reflects the confidence level in the state measurement. The simplified approximation to the $\mathcal{H}^\infty$ optimal NPFSI (noise-perturbed full-state information) estimator, referred to as the reduced-order NPFSI estimator, was given in [4] as follows:

$$\dot{\hat{\theta}}_\gamma = \varepsilon^{-1}\Sigma_\gamma^{-1}A(y,u)^T(y-\hat{x}), \quad \hat{\theta}_\gamma(0) = \bar{\theta}_0, \qquad (3)$$

where

$$\dot{\hat{x}} = A(y,u)\hat{\theta}_\gamma + b(y,u) + \varepsilon^{-1}(y-\hat{x}), \quad \hat{x}(0) = \bar{x}_0,$$
$$\dot{\Sigma}_\gamma = A(y,u)^T A(y,u) - \gamma^{-2}Q(y,u), \quad \Sigma_\gamma(0) = Q_0.$$

In the above, γ represents an attenuation factor that can be tuned to improve estimator convergence. It is proven in [4] that if the system under consideration satisfies a suitable persistency of excitation condition and ε is sufficiently small, the state of (3) converges to the true parameters.

Although the NPFSI technique does not require state derivative information, it does depend on measurement of the full state vector. While the position states x_1 and x_3 are measured directly using optical encoders, the velocity states x_2 and x_4 are not measured. To overcome this problem, we use high-gain observers to estimate x_2 and x_4. The estimation errors are accounted for, in the parameter identification procedure, by the assumption that a noisy measurement of the states is available. Further, to guarantee persistency of excitation, we employ two PID regulators for the control inputs i_d and i_q to independently make the horizontal and vertical dynamics track a suitable reference signal made of a summation of sinusoids at various frequencies[2].

---

[2]Clearly, because the horizontal and vertical dynamics of the system are not decoupled (see (1)), PID control does not yield good tracking performance. However, since at this stage we only focus on the generation of persistently exciting reference signals for parameter estimation, tracking accuracy is not a concern.

With the above in place, the only remaining issue is the choice of the NPFSI parameters γ and ε. It was found through successive experimentation that choosing $\gamma \simeq 1.1$ and $\varepsilon \simeq 0.01$ produced good parameter convergence.

The estimator structure in (3) is used, in what follows, in three different ways. First, to verify the horizontal dynamics. Second, to estimate C_2, C_3, and C_4 and verify the vertical dynamics. Lastly, to estimate $C_1, \ldots C_4$ and simultaneously verify horizontal and vertical dynamics. This is explained in detail in the next section.

V. MODEL VERIFICATION PROCEDURE

With a model of the 2-DOF magnetic levitation system in place along with a technique to estimate the physical parameters, the next task is to develop a procedure capable of verifying the accuracy of said model in predicting the behavior of the actual magnetic levitation system.

A. Verification of Horizontal Dynamics

If the air-gap of the magnetic levitation system is fixed to a constant value $\bar{x}_1$, then the horizontal dynamics from (1) (or (2) equivalently) can be isolated

$$\begin{aligned}\dot{x}_3 &= x_4, \\ \dot{x}_4 &= -L_1(\bar{x}_1)u_1.\end{aligned} \qquad (4)$$

Since at a fixed air-gap $\bar{x}_1$ the L_1 term is constant, the horizontal position x_3 can be solved easily

$$x_3(t) = -\frac{1}{2}L_1(\bar{x}_1)u_1 t^2 + x_3(0). \qquad (5)$$

Note that an initial horizontal velocity of zero is assumed. Equation (5) tells us that if a constant u_1 is applied to the system when the air-gap is fixed, the horizontal position of the mover exhibits a parabolic response. By recording the horizontal position information subject to these conditions, it should therefore be possible to curve-fit a parabola to the data points and obtain an estimate of $L_1(\bar{x}_1)$ at the air-gap in question (and therefore an estimate of the horizontal acceleration of the mover). Such estimate is compared to the value of $L_1(\bar{x}_1)$ obtained applying the NPFSI estimator to (4). This idea is summarized below.

- The motion of the system is constrained (by hardware) to lie on the horizontal axis.
- Position data are collected corresponding to different air-gap values $\{\bar{x}_1^1, \ldots, \bar{x}_1^k\}$.
- A set of parabolas is fitted to horizontal position data at various air-gaps $\{\bar{x}_1^1, \ldots, \bar{x}_1^k\}$ in order to obtain an estimate of $L_1(\bar{x}_1^i), i = 1, \ldots k$ by means of (5).
- For each air-gap $\bar{x}_1^i$, the NPFSI estimator (3) is applied to (4) to estimate $L_1(\bar{x}_1^i)$ and the results are compared.

Figure 3 shows a few examples of the data points obtained and the parabolas that were fitted. Note how the parabolic curves closely approximate the position data, demonstrating the correctness of the horizontal dynamics model (4). Air-gap values here range between 10 and 27.5 mm at 2.5 mm intervals. In each case, the mover is started
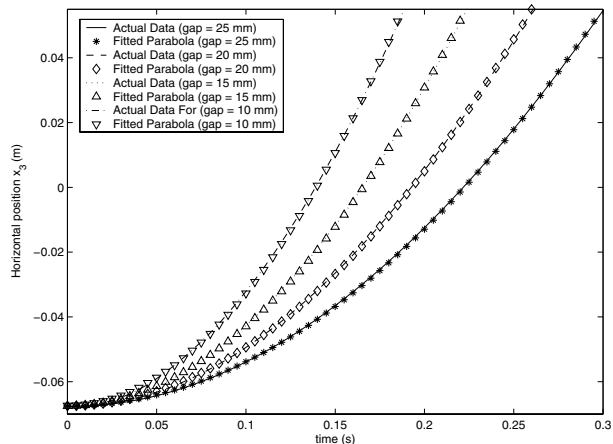
Fig. 3. Some results of parabolic curve-fitting to position data

near $x_3 = -50$ mm and accelerated to about $x_3 = 50$ mm using a current of $u_1 = -0.5$ A.

Figure 4 compares $L_1(\bar{x}_1^i)$ estimates obtained from parabolic curve-fitting and the NPFSI estimator.

The results demonstrate that two different estimation techniques have predicted a similar response for the horizontal dynamics of the magnetic levitation system. This confirms the effectiveness of the NPFSI technique and shows that the horizontal portion of the model describes the physical behavior of the system to a reasonable degree of accuracy. The estimates obtained for the $\varepsilon = 0.05$ case do exhibit increased divergence, but this would be expected since as the value of ε is increased, the estimator puts less emphasis on the estimation error and as a result, the convergence performance of the estimator worsens.
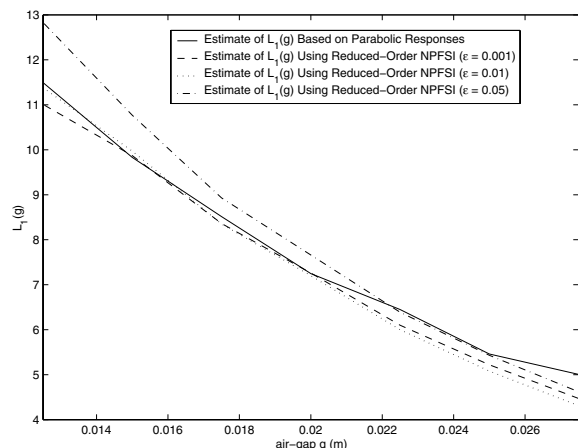

Fig. 4. Comparison of various estimations of $L_1(x_1)$

B. Verification of Vertical Dynamics

To validate the vertical dynamics, we fix the mover at $x_3 = 0$ mm to only allow vertical motion. We also set $u_1 = 0$. The vertical portion of (1) (or (2) equivalently) can

then be isolated

$$
\begin{aligned}
\dot{x}_1 &= x_2, \\
\dot{x}_2 &= G - L_4(\bar{x}_1)u_2^2 - L_3(\bar{x}_1)u_2 - L_2(\bar{x}_1).
\end{aligned}
\tag{6}
$$

From (6), we have that the current $\bar{u}_2$ needed to maintain the air-gap at a desired equilibrium $\bar{x}_1$ is found by solving

$$
G - L_4(\bar{x}_1)u_2^2 - L_3(\bar{x}_1)u_2 - L_2(\bar{x}_1) = 0. \tag{7}
$$

If the model (6) associated with the vertical dynamics is correct, the equilibrium current $\bar{u}_2$ predicted by (7),

$$
\bar{u}_2 = \frac{-L_3(\bar{x}_1) - \sqrt{L_3^2(\bar{x}_1) - 4L_4(\bar{x}_1)(L_2(\bar{x}_1) - G)}}{2L_4(\bar{x}_1)}, \tag{8}
$$

should be close to the measured equilibrium current. The validation procedure for the vertical dynamics is now clear.

- The motion of the mover is constrained (by hardware) to lie on the vertical axis at $x_3 = 0$ mm.
- Set $u_1 = 0$.
- For air-gaps in the set $\{\bar{x}_1^1, \ldots, \bar{x}_1^k\}$, the corresponding equilibrium currents $\{\bar{u}_2^1, \ldots, \bar{u}_2^k\}$ are measured.
- The NPFSI estimator is applied to (6) to estimate the constants C_2, C_3, and C_4 and obtain L_2, L_3, and L_4.
- The terms L_2, L_3, and L_4 are used to determine the *theoretical* equilibrium currents by means of (8).
- The theoretical equilibrium currents are compared to the measured currents.

We choose the air-gap values to range between 10 and 25 mm with 1 mm increments. The NPFSI estimator is applied for three different values of ε. The estimation results are summarized in table II.

TABLE II
VERTICAL MODEL PARAMETERS AT FIXED HORIZONTAL
POSITION USING REDUCED-ORDER NPFSI ESTIMATOR

Parameters	$\varepsilon = 0.001$	$\varepsilon = 0.01$	$\varepsilon = 0.05$
C_2	790.97	791.00	788.98
C_3	30.47	30.90	32.44
C_4	0.11	0.12	0.18

In Figure 5 the theoretical equilibrium currents found using the parameters $C_2, \ldots C_4$ estimated with $\varepsilon = 0.01$ are compared to the measured equilibrium currents.

From the plot, It is clear that while the model begins to diverge from the physical measurements for air-gaps smaller then 15 mm, within the range between 15 and 25 mm the model accurately describes the behavior of the magnetic levitation system. The results therefore validate the vertical dynamics of the model within the range of 15 and 25mm and further validates the NPFSI technique.

The divergence below 15 mm is most likely the result of uncertainties that are not taken into account within the model. In what follows, evidence is provided that suggests the cogging force accounts for most of the uncertainty.
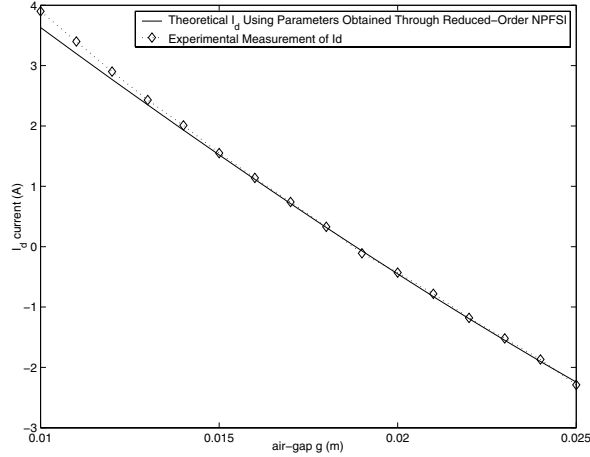
Fig. 5.   Comparing measured i_d currents and the theoretical predictions

C. Analysis of the cogging force

We now seek to determine the source of the discrepancy, observed in Figure 5, between theoretical and measured equilibrium currents at air-gaps smaller than 15 mm.

The cogging force of a linear synchronous motor is defined in [5] to be the force produced by the interaction between the teeth of the stator and the edges of the permanent magnets of the mover. It is a periodic function of the horizontal position of the mover over the slot pitch of the stator. Equation (9) provides a good mathematical representation of this cogging force F_x^c

$$F_x^c = \xi(x_1) \sin\left(\frac{\pi}{t_1} x_3\right). \tag{9}$$

The function $\xi(x_1)$, representing the peak magnitude of the cogging force, is typically inversely proportional to the air-gap x_1, meaning that the cogging force gets stronger as the mover gets closer to the stator. Notice that the peaks of the cogging force occur at odd integer multiples of $t_1/2 = 9.525$ mm. Hence, if the mover is held at the position $x_3 = 28.575$ mm$= 3t_1/2$, then the total normal force exerted by the PMLSM on the surface of the mover is given by

$$F_n(x_1)\Big|_{x_3=3t_1/2} = K_2(x_1)+K_3(x_1)u_2+K_4(x_1)u_2^2+\xi(x_1)$$

where, as before, we are setting $u_1 = 0$. On the other hand, when $x_3 = 0$ mm, the cogging force vanishes and thus the normal force should accurately be represented by

$$F_n(x_1)\Big|_{x_3=0} = K_2(x_1) + K_3(x_1)u_2 + K_4(x_1)u_2^2.$$

Since the unknown constants C_2, C_3, and C_4 in the functions K_2, K_3, and K_4 have already been estimated in the previous section, to estimate $\xi(x_1)$ we let $\hat{K}_2(x_1) = K_2(x_1) + \xi(x_1)$, estimate $\hat{K}_2$ and get $\xi(x_1) = \hat{K}_2(x_1) - K_2(x_1)$. This simple idea is the basis of the next procedure.

- The mover is constrained to lie on the vertical axis at $x_3 = 28.575$ mm$= 3t_1/2$.

- The constants C_3 and C_4 are assumed to be known and equal to the values estimated in the previous section. The constant C_2 is assumed to be unknown and is estimated by applying the NPFSI estimator to (6).
- The value of C_2 just found is used to generate an approximation of $\hat{K}_2(x_1)$ as

$$\hat{K}_2(x_1) = C_2\tilde{\lambda}(x_1)B_{pmy1}(x_1)^2.$$

- The difference $\hat{K}_2(x_1) - K_2(x_1)$ represents an estimate of the *peak cogging force* as a function of the air-gap.

Applying the above procedure and using $\varepsilon = 0.01$ in the NPFSI estimator we get $C_2 = 769.99$. This gives the estimate of $\xi(x_1)$ depicted in Figure 6. This clearly illustrates that the estimated peak cogging force is appreciable (greater than 1 N) when the air-gap is smaller than 15 mm, and otherwise negligible for larger air-gaps.

This is confirmed in Figure 7, where the theoretical equilibrium currents are compared with the actual measurements of u_2 with and without the horizontal offset. While the two predictions are almost identical over most of the air-gap range, they diverge at air-gaps smaller than 15 mm.
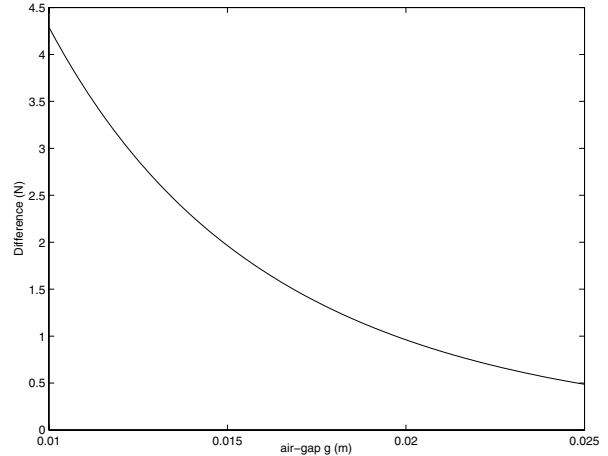

Fig. 6.   Estimate of the peak cogging force over the entire air-gap range

Since the value of the normal force over the range of operation is of the order of 10 N, it is clear from Figure 6 that, within the air-gap range between 15 mm and 25 mm, the cogging force at each horizontal position is a relatively small percentage of the total force, and can be ignored in this range. However, Figure 6 indicates that for smaller air-gaps the discrepancy may become significant.

D. Verification of Complete Model Dynamics

With the horizontal and vertical dynamics of the system verified, the final task is to confirm that all of the model parameters can be estimated simultaneously using the NPFSI estimator and still result in a valid 2-DOF model.

The reduced-order NPFSI estimator is therefore applied across the entire range of operation simultaneously at 3 values of ε, in order to simultaneously estimate the 4 model parameters. The results are provided in table III.
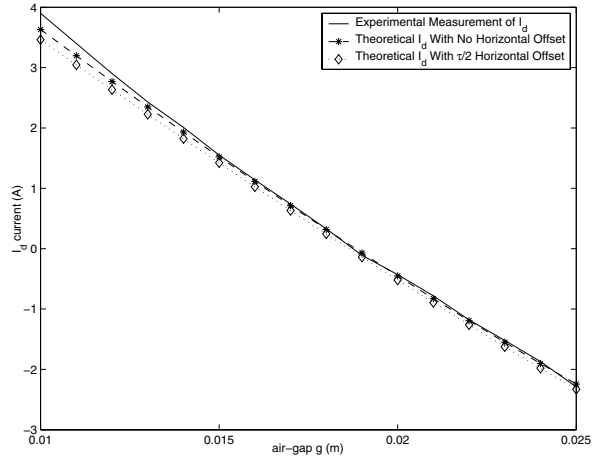
Fig. 7. Measured and theoretical equilibrium i_d currents at each air-gap
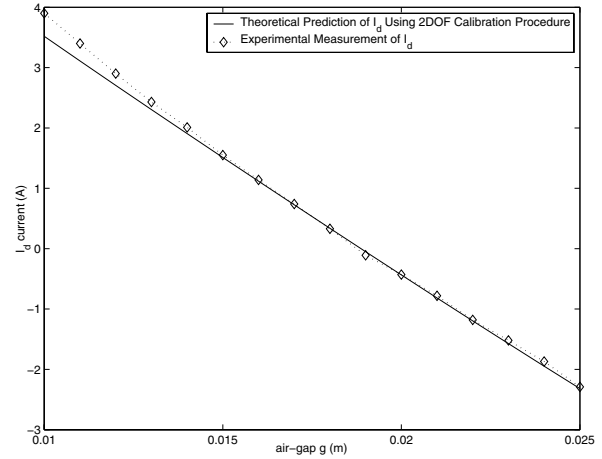
TABLE III
FINAL MODEL PARAMETERS ESTIMATED USING NPFSI

Parameters	$\varepsilon = 0.001$	$\varepsilon = 0.01$	$\varepsilon = 0.05$
C_1	13.97	14.20	16.23
C_2	796.93	796.99	795.01
C_3	30.33	31.04	33.44
C_4	0.06	0.07	0.15

The complete 2-DOF model generated from the above parameter estimates is then verified using the previous horizontal and vertical techniques. Figure 8 compares the estimate of $L_1(x_1)$ generated from the complete model with the estimates obtained at fixed air-gaps, while Figure 9 compares the predicted currents u_2 from the complete model with the actual measurements.
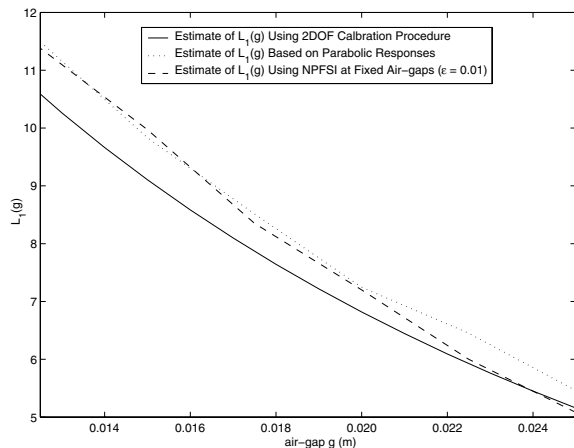

Fig. 8. Comparison between various estimates of $L_1(g)$

The comparisons show that the model generated using the full-span NPFSI estimator describes the behavior of the system to a reasonable degree of accuracy over the desired air-gap range. It should be noted that the horizontal dynamics produced by the 2-DOF calibration procedure appear to diverge from what was estimated in the fixed air-

Fig. 9. Comparing predicted i_d current with actual measurement

gap case. This indicates that the decoupled estimates may be more accurate or that there was not sufficient persistency of excitation. As a result, elements of both the full parameter estimator and the fixed air-gap estimator will serve as the 2-DOF calibration procedure in future control experiments.

VI. CONCLUSIONS AND FUTURE WORK

The model verification results in this paper have shown that when a calibration procedure derived from the work presented in [4] is applied to a realization of a PMLSM-based 2-DOF magnetic levitation system, the state-space model from (1) can accurately predict the behavior of the physical system in an air-gap range between 15 and 25 mm and an horizontal range between -50 mm and 50 mm.

For air-gap values any smaller then the 15mm limit, the effects of uncertainties such as the cogging force become significant and require representation within the modelling.

These results show promise for the remaining part of the work which entails implementing the nonlinear control design developed in [3] on the 2-DOF device presented here as well as on a 3-DOF device under construction.

VII. ACKNOWLEDGMENTS

REFERENCES

[1] K.-Y. Tsai and J.-Y. Yen, "Servo system design of a high-resolution piezo-driven fine stage for step-and-repeat microlithography systems," in *The 25th Annual Conference of the IEEE Industrial Electonics Society*, vol. 1, 1999, pp. 11–16.
[2] W. Kim and D. Trumper, "High-precision levitation stage for photolithography," *Precision Engineering*, vol. 22, pp. 66–67, 1998.
[3] M. Maggiore and R. Becerril, "Modeling and control design for a magnetic levitation system," *International Journal of Control*, vol. 77, no. 10, pp. 964–977, 2004.
[4] G. Didinsky, Z. Pan, and T. Basar, "Parameter identification for uncertain plants using $\mathcal{H}^\infty$ methods," *Automatica*, vol. 31, no. 9, pp. 1227–1250, 1995.
[5] R. Cruise and C. Landy, "Reduction of cogging forces in linear synchronous motors," in *IEEE Africon 1999*, vol. 2, 1999, pp. 623–626.